Journal of Environmental Chemical Engineering 13 (2025) 120084

Contents lists available at ScienceDirect

Journal of Environmental Chemical Engineering

journal homepage: www.elsevier.com/locate/jece

Novel carbon-based materials for sustainable water treatment: Perfluorooctanoic acid adsorption and adsorbent regeneration via thermally activated persulfate oxidation

Andrés Sánchez-Yepes [a,*], Ana Paula Ferreira [b,c,d], Aurora Santos [a], Arturo Romero [a], Helder T. Gomes [b,c], David Lorenzo [a]

[a] Departemento de Ingeniería Química y de Materiales. Universidad Complutense de Madrid, Avda. Complutense S/N, 28040 Madrid, Spain
[b] Centro de Investigação de Montanha (CIMO), Instituto Politécnico de Bragança, Campus de Santa Apolónia, Bragança 5300-253, Portugal
[c] Laboratório Associado para a Sustentabilidade e Tecnologia em Regiões de Montanha (SusTEC), Instituto Politécnico de Bragança, Campus de Santa Apolónia, Bragança 5300-253, Portugal
[d] Centro de Química de Vila Real (CQVR), Universidade de Trás-os-Montes e Alto Douro, Quinta de Prados, Vila Real 5000-801, Portugal

ARTICLE INFO

Keywords:
Carbon materials
PFOA
Adsorption efficiency
Regeneration
Circular economy

ABSTRACT

Rapid increases in municipal and industrial waste pose significant environmental challenges, prompting the need for sustainable technologies. This study reports a framework that combines the production of adsorbents with value-added processes to be used in the remediation of water streams polluted by perfluorooctanoic acid (PFOA) as a target compound. This framework is based on adsorption and regeneration cycles using thermally persulfate-activated advanced oxidation process. Carbon-rich waste, including olive pomace and urban plastic residues, was used to synthesize five carbonaceous materials—activated carbon, hydrochar, pyrochar, activated carbon from hydrochar, and carbon nanotubes—via hydrothermal carbonization and pyrolysis. The adsorbents demonstrated PFOA adsorption capacities ranging from 55 to 303 $mg \cdot g^{-1}$, with activated carbon achieving the highest (303 $mg \cdot g^{-1}$) due to its microporous structure. Adsorption equilibrium followed the Langmuir model, while adsorption kinetics were best described by a pseudo-second-order model. Regeneration was performed using thermally activated persulfate at 60°C. Activated carbon recovered over 70 % of its adsorption capacity with lower oxidant consumption, whereas hydrochar and carbon nanotubes exhibited higher oxidant use and greater structural changes. These results underscore the potential of waste-derived carbon materials for sustainable water treatment and circular economy applications, providing effective removal of persistent pollutants like PFOA with great promise.

1. Introduction

The significant increase in the production of urban and industrial wastes has created urgent environmental challenges [1–3]. Developing sustainable technologies to valorise residues is essential to reduce solid waste and minimise environmental impact [4–6]. A promising strategy is transforming solid waste into value-added carbonaceous material (CM). In this context, the pyrolysis of the raw material with high carbon content or other interesting components can be used to develop catalysis [7] and adsorbents [8–12], being raw materials such as olive oil manufacturing process solid wastes [13–15], or plastic urban wastes [9, 16].

Europe is a leading olive oil producer, with over two million tonnes produced in 2022, mainly from Spain, Italy, Greece, and Portugal, with a production of more than 65 % in the case of Spain [17], generating a significant oil mill effluents and olive pomace residues [18], with a high carbon content for CM production [13]. This adsorbent can be obtained by hydrothermal carbonisation (HTC), employing temperatures in the range 180–250 ºC under autogenous pressured [15,19,20], or pyrolysis at high-temperatures (800–1100ºC) employed quartz reactors under inert (N_2) or oxidative (CO_2) atmospheres [13,15]. Similarly, urban plastic waste, projected to exceed six million tonnes daily by 2025 [21, 22], is a carbon source for heterogeneous catalysts [23–26]. The main production process of this CM is chemical vapor deposition (CVD) on a metal catalyst under pyrolysis conditions (800 °C) [24].

The CM derived from the valorisation can be applied in the treatment

* Corresponding author.

https://doi.org/10.1016/j.jece.2025.120084
Received 18 September 2025; Received in revised form 21 October 2025; Accepted 31 October 2025
Available online 5 November 2025

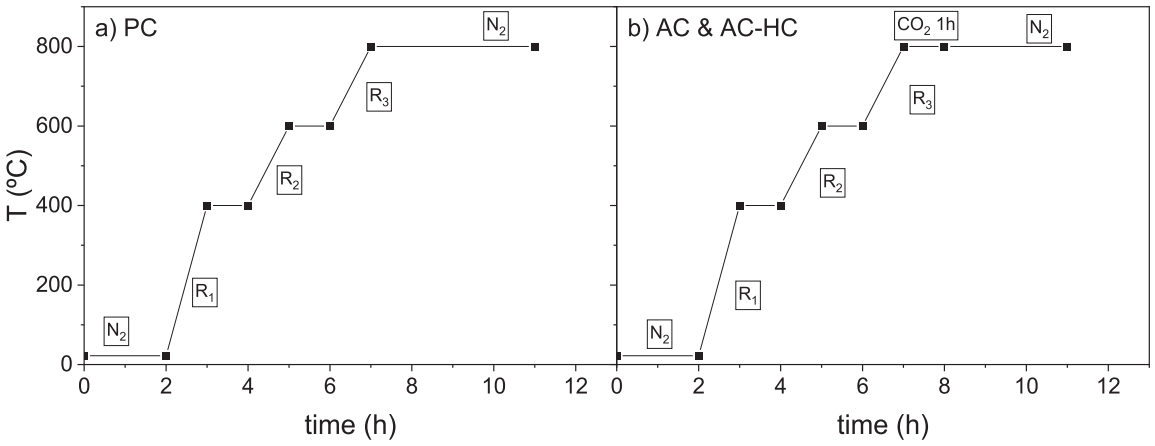

Fig. 1. Temperature ramps used in the a) Pyrochar (PC) and b) Activated carbon (AC) and AC-Hydrochar (AC-HC): pyrolysis process.

of contaminated effluent with persistent organic pollutants (POPs) [27, 28], being an efficient system that allows the remediation of large volumes of wastewater, concentrating the pollutants in the CM [29]. However, the contamination is transferred to the CM, which must be appropriately managed as a residuum in secure landfill cells or incinerated [30–34]. Solvent extraction can recover adsorbents, but additional treatment is required to treat the solvent-contaminant mixture [35]. In this scenario, advanced oxidation processes (AOPs) have emerged as a sustainable alternative to regenerating CMs, removing the adsorbed POPs, promoting their reuse, minimising environmental impacts, and increasing these new CMs circular economy [36–39].

Perfluorinated compounds (PFCs), classified as persistent organic pollutants (POPs), were selected as model contaminants due to their environmental persistence, resistance to degradation, high toxicity, and bioaccumulative properties [40–42]. Perfluorooctanoic acid (PFOA) is one of the most prevalent PFCs in contaminated waters. The key challenge in treating PFOA-contaminated effluents lies in their low concentrations, which result in significant unproductive losses of reagents (oxidants) during direct degradation in the aqueous phase. In the literature, Santos et al. [41] demonstrated the elimination of PFOA (0.1 mM) and defluorination using thermally activated persulfate (PS) as an AOP in 18 h. However, the process required a high oxidant-to-contaminant ratio (1:530) and a 70 °C activation temperature due to PFOA recalcitrant nature. Hybrid treatment strategies could be a promising solution to overcome this challenge. The proposed approach in this work concentrates PFOA from the aqueous phase onto adsorbent materials and then regenerates the spent adsorbents. This method addresses dilution challenges and enhances sustainability by enabling adsorbent reuse, reducing waste, and improving overall process efficiency while ensuring effective PFOA removal.

Various studies have explored PFOA adsorption from the aqueous phase using carbonaceous materials [43–48]. However, the regeneration of these adsorbents, combined with the simultaneous removal and degradation of PFOA, remains underexplored. Efficient and sustainable regeneration techniques are needed to restore the adsorbent functionality and ensure the complete removal and degradation of the adsorbed PFOA. Thermal-activated PS (TAP) was selected to regenerate the spent CMs saturated in PFOA. PS was catalytically decomposed by heat, generating $SO_4^{\bullet-}$ radicals with a high redox potential (2.6 V) [39,49–52]. TAP has demonstrated potential for regenerating spent CMs. Jatta et al. [49] investigated the regeneration of spent carbon in toluene, achieving a 90 % carbon regeneration when applying a 100 mM PS solution at 80 °C. Sanchez-Yepes et al. [39] achieved a 60 % regeneration of highly saturated commercial granular carbon in chlorinated organic compounds using an initial PS concentration of 166 mM and a 60 ºC. Similarly, Huling et al. [52] studied the regeneration of a spent GAC in MTBE, achieving a recovery more significant than 40 % after a single PS application of 40 $g{\cdot}L^{-1}$ of initial oxidant concentration at 55 ° C. Despite these advancements, limited attention has been given to the structural and functional changes in adsorbents through multiple TAP regeneration cycles. Moreover, no studies have examined the regeneration of activated carbons after the adsorption of highly recalcitrant or halogenated organic pollutants like PFOA.

Given the urgent need to develop robust frameworks for addressing persistent contaminants, this study focuses on the development of sustainable CMs derived from industrial and urban wastes for the adsorption of PFOA. The main objective is to systematically investigate the behavior and application of these materials, including their potential for regeneration. Five novel CMs, synthesized from olive pomace and plastic residues were characterized and evaluated for their efficiency in PFOA adsorption. Following adsorption, the spent materials were regenerated using TAP to assess their recovery capacity, potential for reuse in subsequent cycles, and structural changes resulting from the regeneration process.

2. Experimental section

2.1. Materials

Dried olive pomace residues and High-Density Polyethylene (HDPE) were used to prepare the CM. These wastes were provided by an olive pomace oil extraction industry (Mirabaga) and by the company responsible for the waste management system (Resíduos do Nordeste) in northeastern Portugal. The N_2 and CO_2 of first grade, used in the preparation of the carbon material, were supplied by Air Liquid. A COMERCIAL Fe/Ni catalyst was employed for the carbon nanotube synthesis. HCl, NaOH, and KBr provided by Sigma-Aldrich were used as reagents in the pH point zero charge (PZC) and FTIR characterisations of the different CMs.

Sigma-Aldrich purchased analytical-grade PFOA, $Na_2Br_4O_7{\cdot}10\ H_2O$, phenolphthalein, methylene blue, and chloroform used in the PFOA measurement. Sigma-Aldrich supplied PS. Potassium iodide (KI), and sodium carbonate ($NaHCO_3$) were the reagents used to quantify PS. The concentration of fluoride and short-chain organic acids was determined by ion chromatography. Sodium carbonate, sodium bicarbonate, sulfuric acid, and acetone were all from Sigma-Aldrich.

2.2. Procedure

2.2.1. Preparation of carbon materials

Five CMs were prepared from industrial and urban waste. Hydrochar (HC), Pyrochar (PC), Activated carbon (AC), and AC from Hydrochar (AC-HC) were obtained from olive oil production residues. HDPE was used to prepare carbon nanotubes (CNT) as plastic urban waste. The

Table 1
Experimental conditions carried out with the CM synthetized. The experiments were carried out in batchwise magnetically stirred reactor.

Exp.	Objective	V, mL	[PFOA] mg·L^{-1}	T, ºC	[PS], g·L^{-1}	[CM], g·L^{-1}	Time, h
1	Adsorption 5 CM	10	400	25	0	3a	72
2	PFOA Isotherms	10	350–600	25	0	0.1–5a	48
3	PFOA kinetic	10	600	25	0	5a	48
4	TAP oxidation	50	0	40–80	30	5a	0–6
5	PFOA saturation	50	600	25	0	5a	48
6	CM regeneration	50	0	60	30	5b	24
7	CM resaturation	50	600	25	0	5c	48

a) CM not previously saturated in PFOA.
b) CM previously saturated in PFOA.
c) CM previously regenerated with PS.

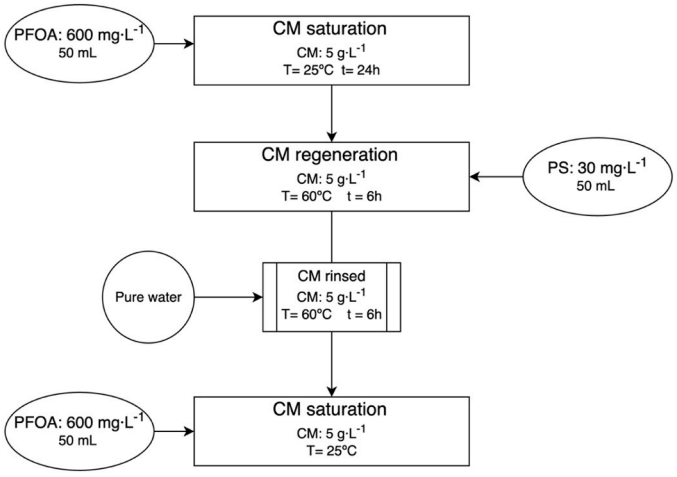

Fig. 2. Experimental workflow (exp. 5, 6 and 7 in Table 1) for evaluating the adsorption and regeneration of carbon materials (CM) for PFOA removal, using persulfate (PS) as an advanced oxidation process (AOP).

procedures for the preparation of these materials is summarized as follows:

Hydrochar (HC): 4 g of dry olive pomace and 30 mL of distilled water were placed in a Teflon reactor, sealed within a steel reinforcement vessel. The reactor was heated in an oven at 230 °C for 3 h to carry out the hydrothermal carbonization process. The resulting hydrochar (HC) was filtered and thoroughly washed with distilled water.

Pyrochar (PC): 10 g of dry olive pomace were placed in a quartz reactor, which was inserted into a temperature-programmed furnace for pyrolysis. To ensure an oxygen-free atmosphere, nitrogen (N_2) was fed into the reactor at room temperature for 2 h. Pyrolysis was carried out under a continuous N_2 flow following a three-step temperature program: Ramp 1: The temperature was increased from ambient to 400 ºC over 1 h and held constant for an additional hour. Ramp 2: The temperature gradually rose from 400 ºC to 600 ºC and maintained for 1 h. Ramp 3: The temperature was increased to 800 ºC and held constant for 4 h. The reactor was then cooled over 12 h under a continuous N_2 flow. The temperature ramps used to produce pyrochar (PC) are schematically represented in Fig. 1a.

Activated carbon (AC) and AC-Hydrochar (AC-HC): 10 g of dry olive pomace were placed in a quartz reactor for the preparation of activated carbon (AC). The same temperature program used for pyrochar (PC) production was applied, with an additional CO_2 activation stage at 800 ºC. Upon reaching 800 ºC, the N_2 flow was switched to CO_2 for 1 h, after which the N_2 flow was reintroduced for an additional 3 h. The temperature ramps used for AC production are schematically shown in Fig. 1b. For AC-HC preparation, 10 g of hydrochar (HC) was used as the raw material and subjected to the same temperature program and CO_2 activation stage as for AC.

Carbon nanotubes (CNT): Carbon nanotubes (CNTs) were synthesized via chemical vapor deposition (CVD) using a Fe/Ni-based catalyst. Specifically, 5 g of high-density polyethylene (HDPE) were combined with a $NiFe_2O_4$ catalyst in a quartz reactor. The pyrolysis process was conducted at 800 °C for 1.5 h under a nitrogen (N_2) atmosphere. Post-synthesis, the resulting material was subjected to reflux in 50 % v/v sulfuric acid (H_2SO_4) at 140 °C for 3 h to leach out any unincorporated Fe/Ni residues.

The materials production yield (Y_{CM}) was calculated by relating the mass of CMs obtained to the mass of raw material used as described in Eq.(1).

$$Y_{CM,i} = \frac{g_{CM,i}}{g_{raw\ material}} 100 \quad i = \{HC, PC, AC, AC-HC\ and\ CNT\} \tag{1}$$

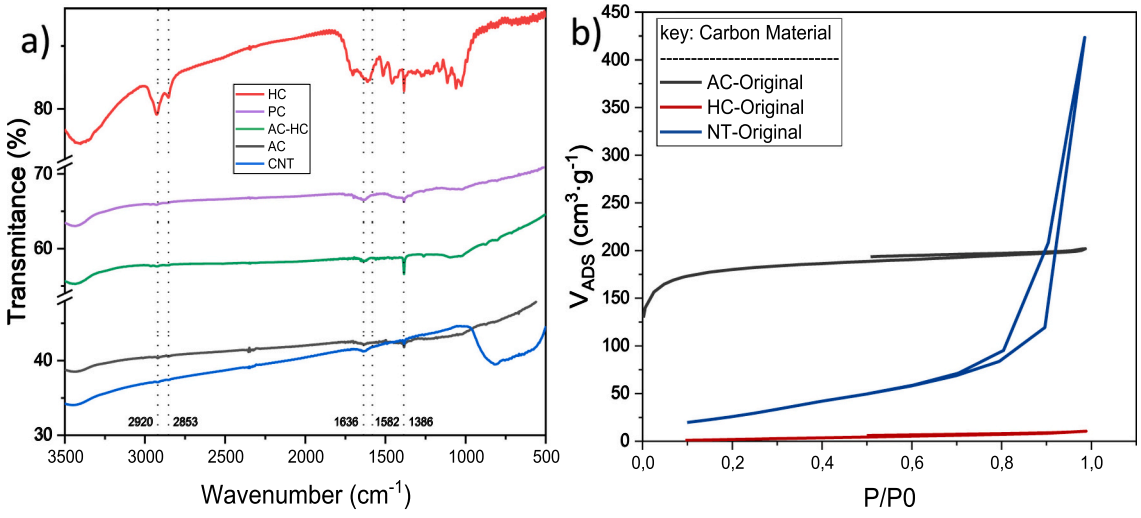

Fig. 3. a) FTIR spectra of the synthesized CMs: HC, PC, AC-HC, AC, and CNT. b) N_2 Adsorption isotherm for original CMs.

Table 2
Characterisation of the structural properties of the synthesised materials.

	S_{BET} ($m^2 \cdot g^{-1}$)	S_{EXT} ($m^2 \cdot g^{-1}$)	V_{MIC} ($cm^3 \cdot g^{-1}$)	S_{MIC} ($m^2 \cdot g^{-1}$)	W_{MIC} ($cm^3 \cdot m^{-2}$)	TPV ($cm^3 \cdot g^{-1}$)
AC	527.3	32.9	0.269	494.39	$2.18 \cdot 10^{-3}$	0.313
HC	13.5	9.8	0.000	3.77	$4.25 \cdot 10^{-4}$	0.016
CNT	118.6	118.6	0.000	0.00	0.00	0.657

Table 3
PFOA Adsorption Capacity of HC, PC, AC, AC-HC, and CNT. Using a $C_{CM,i} = 3\ g \cdot L^{-1}$, $C_{PFOA,0} = 400$ ($pH_0 = 2.66$) $mg \cdot L^{-1}$ and t = 72 h.

CM	pH_f	$C_{PFOA,t}$ ($mg \cdot L^{-1}$)	$q_{PFOA,t}$ ($mg \cdot g^{-1}$)
HC	3.35	292.24	35.92
PC	10.31	400.00	0.00
AC	10.74	74.28	108.37
AC-HC	3.24	400.00	0.00
CNT	2.93	297.54	32.84

2.3. Adsorption experiments

Two sets of experiments were carried out to test the adsorption capacity of PFOA. The msin experimental conditions are summarized in Table 1. In the first set (exp. 1 in Table 1), a vial containing 10 mL of a solution of PFOA (400 $mg \cdot L^{-1}$) was put in contact with 30 mg of the CM (3 $g \cdot L^{-1}$). The vials were magnetically stirred and immersed in a thermostatic bath to maintain the temperature at 25 ± 1 °C during 72 h. The adsorbed amount of PFOA on the CM was calculated with Eq.(2).

$$q_{PFOA} = \left(C_{PFOA,0} - C_{PFOA,t}\right) \cdot V_{aq} / W_{CM,i} \quad i = \{HC, PC, AC, AC-HC, CNT\} \tag{2}$$

being q_{PFOA} ($mg_{PFOA} \cdot g_{CM}^{-1}$) the amount of PFOA adsorbed on CM, $C_{PFOA,0}$ and $C_{PFOA,t}$ ($mg_{PFOA} \cdot L^{-1}$) the initial and final PFOA aqueous

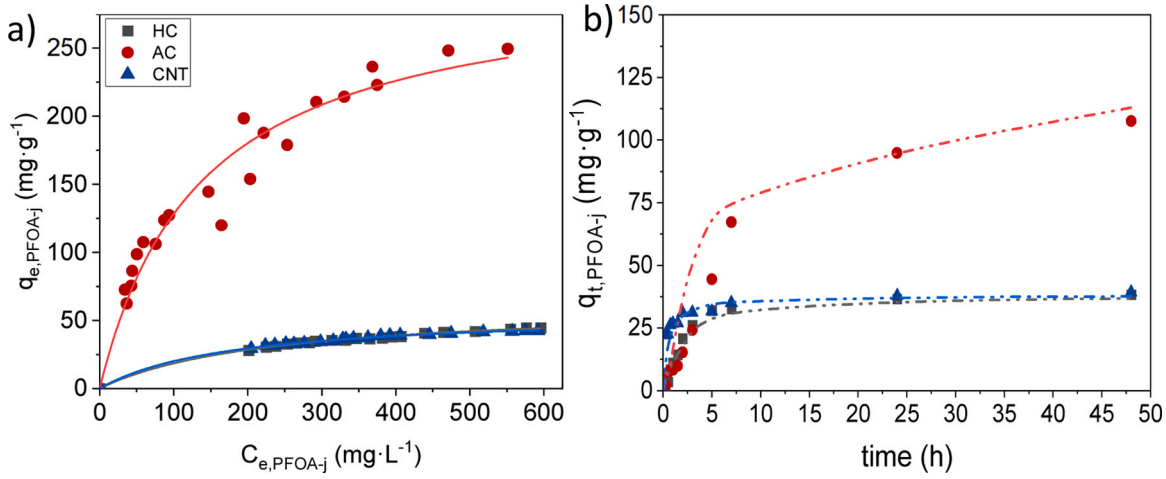

Fig. 4. a) PFOA adsorption isotherms for the HC, AC, and CNT materials, b) PFOA concentration adsorbed on CM: HC, AC, and CNT. $C_{PFOA,0} = 600\ mg \cdot L^{-1}$, $C_{CM} = 5\ g \cdot L^{-1}$, $pH_0 = 2.56$, t = 48 h, 500 rpm, and 25 ° C. Symbols depict experimental values and lines corresponding to predicted values with the PSO adsorption model and the Langmuir isotherm described in Table 4 and Table 5.

Table 4
Parameters Adsorption Isotherms tested and statistical parameters for each CM.

Model	Parameter	HC	AC	CNT
Langmuir	q_m $(mg \cdot g^{-1})$	61.85 ± 1.09	303.12 ± 17.29	55.65 ± 0.72
$q_e = \frac{q_m K_L C_e}{1 + K_L C_e}$	$K_L \cdot 10^3 (L \cdot mg^{-1})$	4.25 ± 0.19	7.33 ± 1.07	5.63 ± 2.22
	R^2	0.996	0.958	0.997
Freundlich	$K_F \left(mg^{1-\frac{1}{n}} \cdot L^{\frac{1}{n}} \cdot g^{-1} \right)$	3.69 ± 0.23	15.64 ± 2.29	5.35 ± 0.39
$q_F = K_F C_e^{1/n}$	$n(-)$	2.55 ± 0.07	2.22 ± 0.13	3.05 ± 0.11
	R^2	0.994	0.946	0.994
Javanovic	$q_{mj} \cdot 10^3 (mg \cdot g^{-1})$	4.44 ± 0.16	7.47 ± 0.91	5.25 ± 0.13
$q_e = q_{mj}\left(1 - e^{K_j \cdot C_e}\right)$	$K_j \cdot 10^{-2} (L \cdot mg^{-1})$	0.47 ± 0.07	2.38 ± 0.11	0.44 ± 0.04
	R^2	0.993	0.926236	0.997
Halsey	$K_H \cdot 10^3$	4.97 ± 2.89	2.13 ± 1.46	1.87 ± 1.10
$q_e = \exp\left(\frac{\ln K_H - \ln C_e}{n}\right)$	n	3.10 ± 0.16	2.23 ± 0.13	3.37 ± 0.16
	R^2	0.981	0.961	0.989610
Temkin	$b_T \cdot 10^3 (kJ \cdot mol^{-1})$	9.61 ± 1.89	36.76 ± 7.95	9.51 ± 2.76
$q_e = \left(\frac{RT}{b_T}\right) \ln(K_T C_e)$	$K_T\ (L \cdot g^{-1})$	98.36 ± 10.01	29.95 ± 2.65	100.10 ± 14.91
	R^2	0.970	$R^2 = 0.960$	0.936

Table 5
Estimated kinetic parameters obtained by fitting data in Fig. 4b, j = HC, AC, CNT [58,62].

Model	Parameter	HC	AC	CNT
PFO $log(q_e - q_t) = log(q_e) - \frac{k_{a,j}}{2.303}$	$k_{a,j}\cdot 10^2$ (h^{-1})	3.36 ± 0.05	7.62 ± 0.11	5.68 ± 0.08
	R^2	0.839	0.935	0.844
PSO $\frac{t}{q_t} = \frac{1}{k_{a,j}\, q_e^2} + \frac{t}{q_e}$	$k_{a,j}\cdot 10^2$ $\left(g_{CM}\cdot mg_{PFOA}^{-1}\cdot h^{-1}\right)$	0.823 ± 0.012	0.050 ± 0.001	4.03 ± 0.006
	R^2	0.991	0.942	0.999
Elovich Model $q_t = \frac{1}{\beta} ln(\alpha\beta) + \frac{1}{\beta} ln(t)$	α $(mg_{PFOA}\cdot h\cdot g_{CM}^{-1})$	5.02 ± 0.07	1.87 ± 0.03	2152.92 ± 32.29
	β $(g_{CM}\cdot mg_{PFOA}^{-1})$	8.02 ± 0.12	22.48 ± 0.34	3.49 ± 0.05
	R^2	0.921	0.908	0.961
Intra-particle diffusion $q_t = k_{d,j} t^{0.5} + I$	$k_{d,j}$ $(mg_{PFOA}\cdot g_{CM}^{-1}\cdot h^{-1/2})$	5.92 ± 0.09	18.05 ± 0.27	3.66 ± 0.05
	I $(mg_{PFOA}\cdot g_{CM}^{-1})$	6.90 ± 0.10	3.90 ± 0.06	20.21 ± 0.30
	R^2	0.709	0.929	0.514
Modified PSO $log(q_e - q_t) + \frac{q_t}{q_e} = log(q_e) - k_m t$	$k_{m,j}\cdot 10^2$ (h^{-1})	1.63 ± 0.025	2.56 ± 0.038	3.65 ± 0.06
	$q_{e,j}$ $(mg_{PFOA}\cdot g_{CM}^{-1})$	53.31 ± 0.80	96.74 ± 1.45	59.36 ± 0.90
	R^2	0.906	0.833	0.929
Film diffusion model $ln\left(1 - \frac{q_t}{q_e}\right) = -k_{F,j} + A$	$k_{F,j}\cdot 10^1$ (h^{-1})	4.91 ± 0.01	0.79 ± 0.01	9.59 ± 0.11
	$A\cdot 10^1$ $(-)$	−0.77 ± 0.01	−1.75 ± 0.01	−1.31 ± 0.02
	R^2	0.839	0.935	0.844

concentration, V_{aq} (L) the aqueous volume and W_{CM} (g) the mass of each CMs. The five CMs prepared were tested, and the corresponding adsorption capacity was compared for these conditions.

PFOA kinetic adsorption and equilibrium isotherms were evaluated in the second set of experiments using the three CMs (exp. 2 and 3 in Table 1), which showed the best adsorption capacity from the first set. Equilibrium isotherms were determined batchwise, with 10 mL vials containing 10 mL of aqueous solution of initial PFOA concentrations in the range 350–600 mg·L^{-1} and CM loading from 0 (control) to 5 g·L^{-1} . The vials were agitated for 48 h, after which the remaining PFOA concentration in the aqueous phase was measured, and the PFOA adsorbed in CM was calculated by Eq.(2). All experiments were conducted in triplicate to ensure reproducibility. Kinetic adsorption experiments were conducted batchwise with vials but using 600 mg·L^{-1} PFOA solution and 5 g·L^{-1} of the adsorbent material (CM). Vials were and sacrificed at different times, and the remaining PFOA concentration in the aqueous phase was measured.

2.4. Oxidation experiments: thermal activated persulfate (TAP)

Two oxidation experiments were conducted: the first focused on investigating the reaction between the oxidant and the carbonaceous material (CM) without adsorbed PFOA. In contrast, the second examined the interaction between the oxidant and PFOA adsorbed onto saturated CM. The experimental conditions are summarized in Table 1.

The reaction between PS and CM in the absence of adsorbed PFOA (exp. 4 in Table 1), was studied in batch mode at three different temperatures (40, 60, and 80 °C) with a CM loading of 5 g·L^{-1} . A total of 50 mL of distilled water and 0.25 g of CM were placed in a closed 50 mL glass reactor, which was well-mixed and maintained in a thermostatic bath (IKA 7 mixing plate with PID temperature controller) to ensure a constant temperature and adequate mixing of the aqueous phase. Once the target temperature was reached, PS was added to the aqueous phase to achieve an initial concentration of 30 g·L^{-1} , marking the start of the reaction (time zero).

The reaction between PS and the spent CMs after PFOA adsorption was investigated as follows (exp. 5, 6 and 7 in Table 1). The experimental woflow carried out in this experiment is summarized in: First, the CMs were saturated with PFOA by contacting 0.5 g of each CM with 50 mL of a 600 mg·L^{-1} PFOA solution for 48 h. After PFOA saturation, the CMs were filtered, and the residual PFOA concentration in the aqueous phase was measured to calculate the amount of PFOA adsorbed using Eq.(2). Saturated CMs were then air-dried for 24 h. Afterwards, the spent CMs were regenerated batch-wise using thermally activated persulfate (TAP) using the same procedure previously described in the absence of PFOA in the CM. The PS concentration in the aqueous phase was monitored over time during 6 h in all the runs. Samples of 0.25 mL were collected at regular intervals.

The regenerated CM was recovered and washed in 50 mL of milli-Q water for 2 h at 60 ° C. Then, 0.25 g of regenerated CM was placed in contact with 50 mL of fresh PFOA solution (600 m g·L^{-1}). After 48 h of contact, the remaining PFOA concentration in the aqueous phase was measured, calculating the amount of PFOA adsorbed, $q_{PFOA,re\text{-}saturated}$, by Eq.(2). The efficiency of the regeneration step was calculated using the recovered adsorption capacity (RAC) defined in Eq.(3)

$$RAC = q_{PFOA,re-saturated} / q_{PFOA-initial} \cdot 100 \quad (3)$$

being $q_{PFOA\text{-}initial}$ and $q_{PFOA,re\text{-}saturated}$ ($mg_{PFOA}\cdot g_{CM}^{-1}$) the amount of PFOA adsorbed in the original CM and after TAP regeneration, both at equilibrium conditions.(Fig. 2)

2.5. Analytical methods

2.5.1. Characterisation of the carbon materials

The PZC for the synthesised CM, was assessed via the pH drift method [53]. Specifically, 75 mg of powdered of each CM was combined with 10 mL of 0.01 M NaCl solution in glass flasks, with the initial pH adjusted between 2 and 10 using 0.1 M HCl or NaOH. The mixtures were agitated and equilibrated for 24 h at 300.15 ± 2 K. The final pH was recorded, and the PZC was defined as the pH point remaining constant post-equilibration. Each trial was conducted in triplicate under controlled laboratory conditions utilizing triple distilled water to

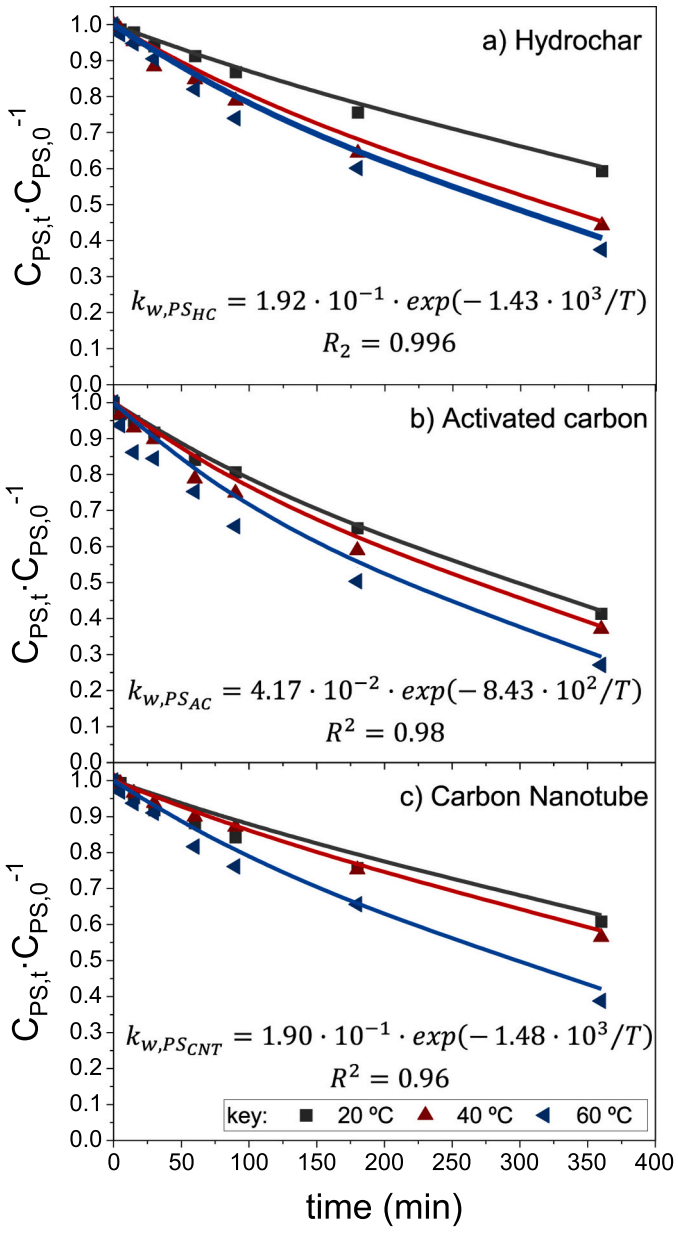

Fig. 5. Remaining PS with a) HC, b) AC, and c) CNT. $C_{CM,j}$= 5 g·L^{-1}, C_{PS}= 30 g·L^{-1}. Symbols depict experimental values, and lines simulate predicted values using the kinetic PS consumption model in, the kinetic constants are provided in the equations of the Figure.

mitigate background conductivity. Eleven magnetically steering vials containing 7.5 g·L^{-1} of the CM and 10 mL of NaCl (0.01 M) solution were prepared for each material. The initial pH of each vial was adjusted between 2 and 12 with HCl (0.1 M) and NaOH (0.1 M). The vials were agitated, and the pH was measured after 24 h. The final pH values were compared with the initial pH values of the different adjusted NaCl solutions.

The porous texture of the CM was characterised by adsorption-desorption of N_2 at −196 °C in a Quantachrome instrument NOVA TOUCH LX4 quantum instrument (Quantachrome Instruments, Florida, USA). The samples were outgassed at 150 ° C for 8 h. From this data the apparent surface area (SBET, m2·g-1) the external surface area (S_{EXT}, m^2·g^{-1}) and the micropore volume (V_{MIC}, cm^3·g^{-1}) were obtained.

The Fourier-transform infrared spectroscopy (FT-IR) was obtained by Perkin Elmer FT-IR spectrophotometer UATR Two, with a resolution of 4 cm^{-1} and scan range of 3500 – 500 cm^{-1}.

The concentration of PFOA in the aqueous medium was measured by spectrophotometry using methylene blue as an indicator. Given the surfactant nature of PFOA [42,54], it was analysed using the methodology developed by Jurado et al. [55]. Three solutions were used for the measurement of PFOA: Buffer I: 1 L $Na_2B_4O_7$·10 H_2O (50 mM adjusted to pH 10.5 with NaOH), buffer II: 3.13 mM methylene blue in 100 mL $Na_2B_4O_7$·10 H_2O (10 mM adjusted to pH 5.5) and 100 mL phenolphthalein (1 g·L^{-1} in ethanol). In 5 mL of aqueous sample with PFOA, 200 µL of buffer I, 50 µL of phenolphthalein and 100 µL of Buffer II were added. A liquid extraction was performed with 4 mL of chloroform, and the absorbance of the extract was measured in a UV–vis spectrum (UV–VIS Spectrometer, T70, PG Instrument Ltd., Lutterworth, UK) at 650 nm wavelength.

The concentration of PS was determined by colorimetric titration using an indicator solution of KI (100 g·L-1) and NaHCO3 (5 g·L-1). Ionic organic by-products, such as fluorides, were measured by ion chromatography (Metrohm 761 Compact IC) with anionic chemical suppression and a conductivity detector. The pH was measured with a Basic 20-CRISON pH electrode.

3. Results and discussions

3.1. Carbon materials: production and characterisation

3.1.1. Carbon material production yield

The production yields of the five CM calculated with Eq. (1). HC was the CM with the highest $Y_{CM,}$ losing 50 % of the initial row material due to removing natural oils in the olive pomace in the hydrothermal carbonisation. AC, PC, and AC-HC were the pyrolysis materials with the lowest Y_{CM} (25 %), associated with the burn-off solid effect. In the case of AC-HC, the 25 % Y_{CM} obtained was associated with a prior 50 % loss of row material during HC preparation. The Y_{CM} for the CNTs obtained was 35 %. This value was obtained by considering the percentage of burn-off from the CVD pyrolysis and the weight lost in the acid-washing step.

3.1.2. Carbon material characterization

The CM synthesised was characterised by measuring the PZC pH, identifying the main functional groups on the CM surface by FTIR, and analysing the structural properties, such as specific surface area and pore volume.

The PZC of the CM prepared was determined using the experimental values. HC and CNT presented a PZC pH < 7, meaning the surface of these materials was positively charged, attracting anions from the medium and donating protons (H+), acidifying the solution. For the rest of the materials, AC, PC, and AC-HC, the PZC-pH was higher than 7 since the surface of these CMs presented a negatively charged surface and was more likely to attract protons and donate OH-.

FTIR spectra of the CMs are represented in Fig. 3. The bands in the spectrum of HC are more defined than the rest of the CMs prepared. It was attributed to the colour of the HCs final product (light brown), which was lighter than the rest of the CM synthesised (dark black), making it more suitable for FTIR analysis. Spectra are inherently limited by the highly graphitic nature and low infrared absorbance of these materials, which results in weak or overlapping signals. HC presented bands located at 2920 and 2853 cm^{-1} related to the symmetric and asymmetric stretching vibration of the CH bonds, which indicate the -CH_2 groups and aliphatic hydrocarbons on the carbon surface [26,56]. HC also presented bands around 1580 cm^{-1} associated with C═C bonds, which are typical of aromatic rings, indicating graphitic structures within the carbon material, while bands around 1620 cm^{-1} are associated with the stretching vibrations of the olefinic groups of the carbonaceous materials. Between 1700 and 1300 cm^{-1}, vibrations were attributed to the bending of O-H group, as observed at 1386 cm^{-1} [56, 57]. AC, PC, and AC-HC presented similar low-resolution trends of the bands associated with C-H and C-O groups due to the higher C content

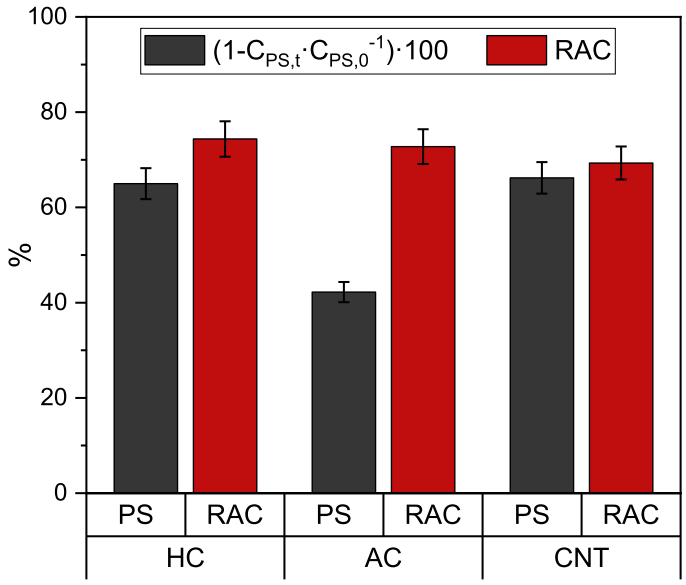

Fig. 6. Experimental results of a) Recovery adsorption capacity (RAC, Eq.(3)) and b) PS consumption. Maintaining $C_{CM} = 5$ g·L^{-1}, $C_{PS,0} = 30$ g·L^{-1} and PS activation temperatures: 60 ° C and 360 min of reaction.

Table 6
Final pH, and theoretical versus experimental sulfate and fluoride ions concentrations in the aqueous reaction medium.

		Theorical		Experimental	
Material	**pH$_f$**	**Sulfates (g·L^{-1})**	**Fluorides (g·L^{-1})**	**Sulfates (g·L^{-1})**	**Fluorides (g·L^{-1})**
HC	3.24	10.50	95.81	9.38	55.2
AC	10.28	17.40	286.12	16.89	206.64
NT	2.86	10.14	94.40	8.75	38.28

due to the pyrolytic process [26]. These bans were also observed in the CNT spectrum. CNT showed a depression between the 1000 and 500 cm^{-1} bands corresponding to the Fe and Ni residues that are part of the catalyst used in the CVD.

In the FTIR spectra, the presence of bands associated with oxygen-containing groups (–OH, –COOH, –C═O, –C–O–) indicates the existence of active sites that can interact with PFOA through hydrogen bonding or electrostatic interactions. For example, the broad band around 3400 cm^{-1} , attributed to hydroxyl groups, and the signals in the 1700–1720 cm^{-1} region, corresponding to carbonyl or carboxyl groups, are desirable features that favour adsorption of the polar end of PFOA [26,67].

In more hydrophobic carbonaceous materials, such as carbon nanotubes or activated carbons treated at high temperatures, the bands related to oxygenated groups are usually less intense, but peaks associated with aromatic C═C bonds can be observed, which promote π–π interactions with the PFOA chain. This type of hydrophobic and van der Waals dispersion interaction becomes relevant when the dominant adsorption mechanism is governed by affinity between nonpolar regions [26].

In the case of Hydrochar, which retains a higher amount of oxygen-containing functional groups due to its lower degree of carbonization, FTIR spectra show more pronounced signals in the 1000–1300 cm^{-1} (C–O) and 1600–1700 cm^{-1} (C═O) regions. These groups increase surface polarity and can enhance PFOA adsorption in aqueous media through electrostatic interactions between the carboxylate end of the contaminant and the protonated surface groups of the material [26,67].

The structural characteristics of the CMs are summarised in Table 2, and the adsorption isotherm is represented in Fig. 3b. From the analysis, the specific surface area (S_{BET}, m^2·g^{-1}), external surface area (S_{EXT}, m^2·g^{-1}), micropore surface area and the volume (S_{MIC}, m^2·g^{-1} and V_{MIC}, cm^3·g^{-1}respectively), the ratio between the micropore volume and surface area (cm^3·m^{-2}) and the total pore volume of the material (TPV, cm^3·g^{-1}) were obtained.

The CM with the highest surface area was AC, as shown in Table 2. With a predominantly microporous structure, over 93 % of its total surface area and 86 % of its total pore volume (TPV) are attributed to micropores. In contrast, HC and CNT exhibited significantly smaller surface areas, with HC presenting only 13.58 m^2·g^{-1} . The external surface area dominates for these two materials, especially in CNT, where the entire measured area is external. The latter can be explained taking that it is mainly due to their tubular structure with graphitic walls and nanometric inner cavities, which are often partially blocked or inaccessible because of impurities, residual catalysts, or closed tube ends formed during synthesis. The thermal treatment applied during CNT production also plays an important role reducing, oxygen-containing functional groups and structural defects, increasing the degree of graphitization and reducing the number of active sites within the inner walls or defect regions [24].

Reliable surface area measurements could not be obtained for pitch-based carbon (PC) and the composite AC-HC. In both cases, the estimated values were very low (below 10 m^2·g^{-1}), preventing a viable result from being recorded.

As shown in Fig. 3b, the adsorption isotherm for AC corresponds to Type I, which is characteristic of microporous materials [58,59], aligning with the values presented in Table 2. In contrast, HC and CNT exhibit adsorption isotherms closer to Types II and III, typically associated with macroporous materials and strong or weak adsorbate interactions [58,60]. Although the CNT AD was classified as type III according to the IUPAC classification. This decision is based on the overall shape of the isotherm, which lacks a defined plateau and shows a continuous increase in adsorption at higher relative pressures, indicating weak adsorbate–adsorbent interactions. The small hysteresis observed can be attributed to textural effects such as interparticle voids or narrow slit-like spaces between aggregated nanotubes, rather than to a true mesoporous network typical of type IV materials [58,60]. Table 2 further confirms that these materials possess virtually no microporous surface area.

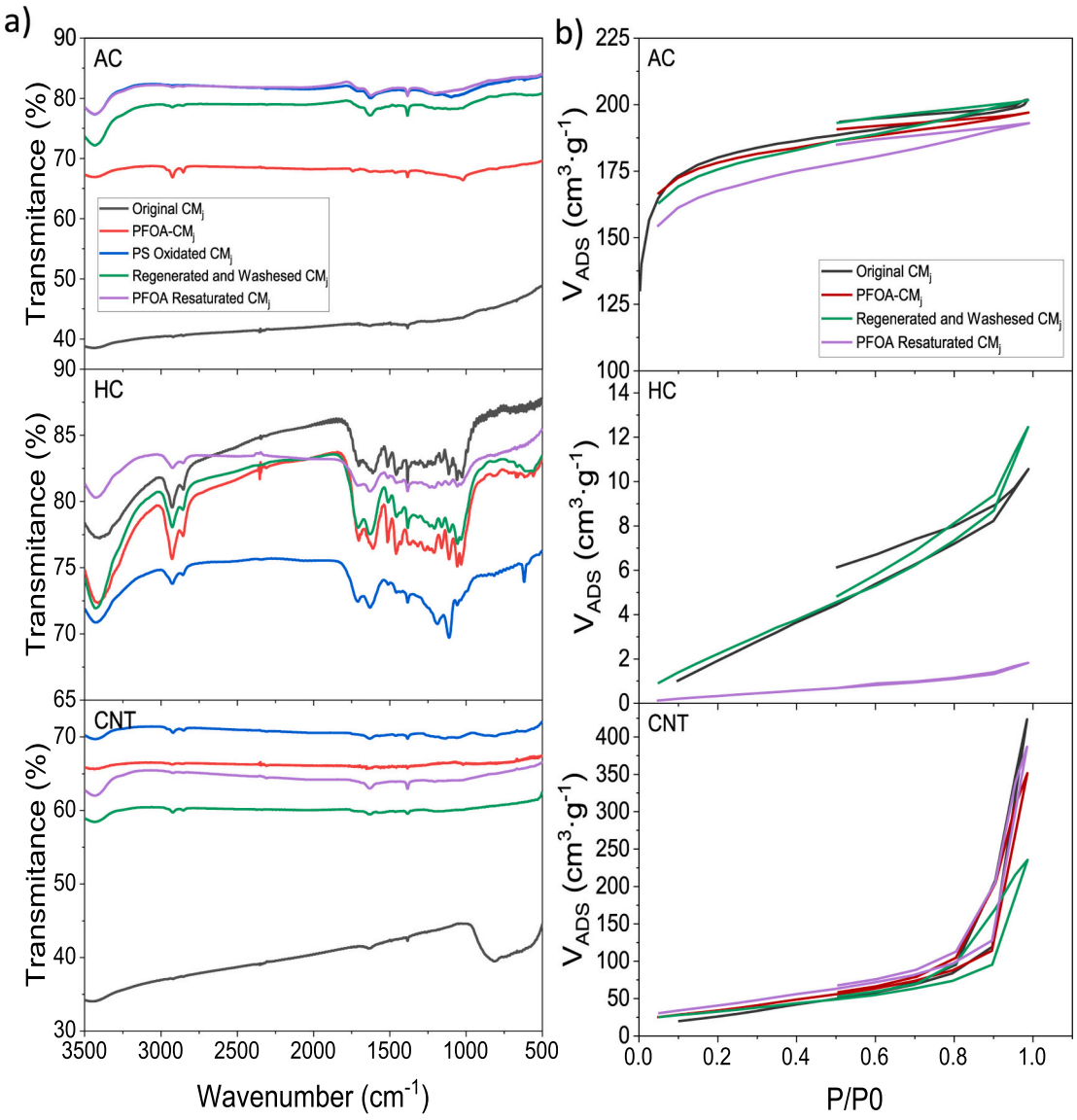

Fig. 7. a) FTIR analysis after regeneration with TAP b) N_2 Adsorption isotherm for original CMs, CMs after saturation in PFOA, after regeneration with TAP and after saturation up) AC, centre) HC and down) CNT.

Table 7
Structural changes in the CM samples tested after regeneration with TAP.

	S_{BET}	S_{EXT}	S_{MIC}	TPV	V_{MIC}	$W_{MIC}\cdot10^3$
	($m^2\cdot g^{-1}$)	($m^2\cdot g^{-1}$)	($m^2\cdot g^{-1}$)	($cm^3\cdot g^{-1}$)	($cm^3\cdot g^{-1}$)	($cm^3\cdot m^{-2}$)
Original AC	527.31	32.92	494.39	0.313	0.269	2.180
PFOA-AC	518.04	26.17	491.87	0.305	0.265	2.160
Regenerated and Washed AC	513.53	29.46	484.06	0.312	0.267	2.210
PFOA Resaturated AC	489.37	24.23	465.13	0.299	0.262	2.250
Original HC	13.58	9.81	3.76	0.016	> 1	0.425
Regenerated and Washed HC	11.69	9.99	1.70	0.015	> 1	0.120
PFOA Resaturated HC	12.18	11.57	0.61	0.014	> 1	0.655
Original CNT	118.66	118.66	0.000	0.657	0.000	0.000
PFOA-CNT	129.79	129.79	0.000	0.545	0.000	0.000
Regenerated and Washed CNT	160.45	160.45	0.000	0.501	0.000	0.000
PFOA Resaturated CNT	149.80	149.80	0.000	0.600	0.000	0.000

3.2. Adsorption of PFOA on synthesised CM

To compare the adsorption capacity of the synthesised CMs, a PFOA concentration of 400 $mg\cdot L^{-1}$ in the aqueous phase and a CM loading of 3 $g\cdot L^{-1}$, was used, measuring the final aqueous PFOA concentrations in the aqueous phase after 72 h of contact. Table 3 summarises the adsorption capacity ($q_{PFOA,t}$), and the final solution pH (pH_f).

Among the tested materials, AC displayed the highest adsorption capacity (108.37 $mg\cdot g^{-1}$), attributed to its large specific surface area. In contrast, adsorption on AC-HC and PC was negligible, likely due to their

low specific surface areas. Consequently, the adsorption equilibrium isotherm and kinetics study were conducted only for AC, CNT, and HC.

Adsorption isotherms for CMs-PFOA with HC, AC, and CNT were evaluated at 25 °C and a contact time of 48 h and represented in Fig. 4. The experimental data were used to fit the parameters of the models presents in Table 4. Statistical evaluation demonstrates that the Langmuir model offers the most accurate representation of the experimental data, as indicated by superior R^2 values across all three CMs. Langmuir isotherms constants were used to predict the concentration of PFOA in both phases. PFOA adsorption kinetics were analysed using experimental data from the adsorption tests. The aqueous PFOA concentration was monitored over time and the adsorbed amount was calculated by Eq.(2) and represented in Fig. 4b. Kinetic model parameters and statistical indicators are summarized in Table 5.

Among the tested models, the pseudo-second-order model (PSO) achieved the best fit. CNTs exhibited the highest kinetic constant, likely due to trace Fe and Ni from the synthesis catalyst, which enhance PFOA adsorption through stronger interactions with the carbon surface, as also reported by Ahn et al. [61].

AC exhibited the highest adsorption rate constant. This result indicates that AC possesses a high affinity for PFOA molecules, which can be attributed to its well-developed microporous structure and the abundance of oxygen-containing surface groups that facilitate electrostatic and hydrogen-bonding interactions with the polar head of PFOA. Although the Langmuir model assumes monolayer adsorption on homogeneous sites, the elevated kinetic constant observed for AC may also reflect the contribution of fast surface adsorption and partial pore diffusion processes.

3.3. TAP oxidation of carbon materials

3.3.1. PS reactivity with unpolluted CM

The reactivity of PS with synthesised CMs (without PFOA adsorbed) was studied at three activation temperatures (20, 40, and 60 ° C), using an aqueous solution of 30 $g{\cdot}L^{-1}$ of PS with CM loading concentrations 5 $g{\cdot}L^{-1}$. As seen in Fig. 5, within the studied temperature range (20–60 ºC), PS decomposed upon contact with the carbon materials (CMs), consistent with the findings of Sánchez-Yepes et al. [62]. For all materials, PS consumption increased with rising temperature. Additionally, materials with larger surface areas exhibited higher oxidant consumption.

At 60 ºC and 360 min, more than 70 % of the initial PS was consumed for AC at both loading concentrations. In contrast, HC and CNT consumed less than 60 % of the initial PS under the same conditions.

The kinetics of PS reaction with HC, AC and CNT without adsorbed pollutants was investigated through the results in Fig. 5. The rate equation for PS decomposition is assumed to follow first-order heterogeneous kinetics

$$-\frac{dC_{PS}}{dt} = k'_W \cdot C_{PS,t} \quad ; k'_w = k_{w_{PS}} \cdot C_{CM,j} \quad (j = HC, AC, CNT) \tag{4}$$

Being $C_{PS,0}$ and $C_{PS,t}$ ($g{\cdot}L^{-1}$) the PS concentration at zero and t time, respectively, k_{wPS} ($L{\cdot}g_{MC}^{-1}{\cdot}h^{-1}$) the heterogeneous kinetic constant for PS decomposition, $C_{CM,j}$ ($g_{CM,j}{\cdot}L^{-1}$) the CM loading of material j and t (h) the reaction time. The rate constant for persulfate decomposition, k_{wPS} is described by the Arrhenius equation:

$$k_{w_{PS}} = k_{w_{PS,0}} \cdot e^{\frac{-Ea}{R \cdot T}} \tag{5}$$

being $k_{wPS,0}$ ($L{\cdot}g_{MC}^{-1}{\cdot}h^{-1}$) the preexponential, factor and E_a the activation energy. Both values were fitted from the experimental results and the values of this parameters are given in Fig. 5 for the 3 CM. Kin the latter, the predicted data are represented as lines. A good agreement between the experimental and predicted PS consumption values validates the kinetic model proposed.

3.3.2. Regeneration of PFOA saturated CMs by TAP

As described in the experimental Section 5 $g{\cdot}L^{-1}$ of each CM material (HC, AC and CNT) were first saturated in PFOA (600 $mg{\cdot}L^{-1}$ aqueous initial concentration). This elevated concentration of PFOA was chosen to assess the practical applicability of the proposed framework and the synthesized CMs for the processes of adsorption and regeneration in the removal of PFOA from aqueous environments. The amount of PFOA adsorbed was calculated using Eq. (2). The saturation of the CMs resulted in 114.24, 39.57 and 37.43 $mg_{PFOA}{\cdot}g_{CM}^{-1}$ for AC, CNT, and HC, respectively.

Saturated CMs were regenerated as described in the experimental section and washed with water to remove the sulfates deposited on the surface of the materials, as previously observed by Sanchez-Yepes et al. [62]. The regenerated materials were saturated in a new PFOA solution, and the RAC was calculated using Eq. (3). The PS consumption in the regeneration step and the RAC values for each CM are represented in Fig. 6.

As shown in Fig. 6, RAC values were consistently above 70 % of the initial adsorption capacity for all three materials, with minimal differences among CMs observed after the thermal activation process (TAP). However, PS consumption differed notably: HC and CNT consumed over 60 % of the initial PS, while AC consumed only 40 %. This finding indicates that AC was the most efficient material, achieving a higher RAC with lower PS consumption. In contrast, HC and CNT were less efficient, as their higher PS consumption did not translate into additional adsorption recovery, rendering a higher PS unproductive consumption.

To further assess regeneration efficiency, the ratio of moles of PS consumed to moles of PFOA removed was calculated. The moles of PFOA removed were determined from the amount of PFOA re-adsorbed after regeneration. The calculated ratios were 131.23, 72.82, and 128.61 $mol_{PS}{\cdot}mol_{PFOA}^{-1}$ for HC, AC, and CNT, respectively. A lower ratio reflects better PS utilisation, indicating that AC exhibited the highest efficiency in TAP regeneration.

The final aqueous reaction medium was analysed for pH and ion concentrations. The concentrations of sulfates and fluorides were compared with theoretical values derived from PS consumption, and the amount of PFOA re-adsorbed after regeneration was assumed to be equivalent to the PFOA removed during regeneration. These results are summarised in Table 6.

Final pH values (Table 6) revealed acidification of the aqueous phase for HC and CNT, which can be attributed to sulfate species generated during PS thermal decomposition. Conversely, the aqueous medium for AC showed a basic pH after regeneration, consistent with its strong negative surface character ($pH_{PZC} = 10.5$). The sulfate species generated during regeneration only slightly reduced this value to 10.28 (Table 6).

A good agreement was observed between experimental and theoretical sulfate concentrations, calculated from PS consumption during TAP regeneration. However, experimental fluoride concentrations were lower than the theoretical values predicted from the amount of PFOA re-adsorbed. This discrepancy suggests that some fluorides may have been retained within the material structure and not released into the aqueous medium. The literature has reported similar behaviour when regenerating activated carbons adsorbing chlorinated compounds [38].

3.4. Carbon materials characterisation after regeneration by TAP

The structural properties of the CMs were analysed after the adsorption and oxidation processes and compared with those of the original materials. FTIR analysis evaluated surface chemistry changes, and the resulting band groups emerging after adsorption or oxidation are shown in Fig. 7a.

HC exhibited the best resolution in the FTIR spectra, likely due to its natural colour. The adsorption of PFOA, both from the saturation step and after regeneration (RAC analysis), resulted in the appearance of new bands. A prominent band at 3422 cm^{-1} corresponds to the -OH hydroxyl group [26], while bands at 1558 and 1380 cm^{-1} are associated with the

symmetric and asymmetric carboxylate groups, respectively [63]. The detection of acid bands at 1720 cm^{-1} (-COOH) and 1380 cm^{-1} ($-COO^-$) further confirms the adsorption of PFOA onto the carbon material. Additionally, a band at 1018 cm^{-1} corresponds to -C-OH groups, indicating carbon oxidation. Bands corresponding to CF-related groups were also observed: CF_3 at 1208 cm^{-1} , CF_2 at 1160 cm^{-1} , and CF at 670 cm^{-1} . [64,65].A slight shift in the bands corresponding to hydroxyl groups (-OH) was observed for all CMs, with the maximum band located at 3500 cm^{-1} [26] after the oxidation process (PS reactivity study and TAP regeneration). Bands associated with the symmetric and asymmetric stretching of aliphatic -CH, CH_2, and CH_3 groups [66] were detected at 2920 and 2853 cm^{-1}. The thermal oxidation of PS introduced oxygen-containing functional groups, which were identified in the FTIR spectra. A band at 1720 cm^{-1} corresponds to C═O vibrations from ketones, aldehydes, and carboxylic acid groups, while a parallel band at 1629 cm^{-1} [66] and an additional band at 1385 cm^{-1} can also be attributed to carboxylic groups (-COOH and $-COO^-$) [26,67] shown at 1385 cm^{-1}. Furthermore, the PS oxidation process generated sulfur-containing groups, as indicated by the S-O stretching band at 1109 cm^{-1} [68,69].

The corresponding N_2 adsorption-desorption isotherms are presented in Fig. 7b, and the summarised structural surface modifications are detailed in Table 7. The adsorption and oxidation processes applied to AC did not alter its isotherm type, confirming the strong stability of its microporous structure. After PFOA adsorption, a slight 1.75 % reduction in the total surface area was observed (Table 7). The external surface showed the most significant decrease (20.5 %), indicating that PFOA adsorption primarily occurred on the AC surface. Changes in micropore volume and total pore volume (TPV) were minimal.

Following TAP regeneration, the N_2 adsorption isotherms (Fig. 7b) and external surface area values (Table 7) were largely restored, demonstrating the successful recovery of the material. During oxidation, sulfate radicals attacked the unoccupied AC surface, oxidising it and losing microporous surface area. However, a further surface area reduction was observed during RAC evaluation due to PFOA re-entering the material surface, as noted in Table 7.

The N_2 adsorption-desorption isotherms for HC are presented in Fig. 7b center. Post-PFOA adsorption, the HC isotherm and structural values could not be obtained due to sample instability during analysis. TAP regeneration of HC successfully recovered the external surface area (Table 7) but led to a significant 54.8 % reduction in the micropore surface. Subsequent re-adsorption of PFOA after regeneration caused an additional micropore surface reduction exceeding 60 %.

Fig. 7b down shows the N_2 adsorption isotherm for CNT, with the corresponding structural properties summarised in Table 5. PFOA adsorption on the CNT surface increased the external surface area and caused a 17 % reduction in the total pore volume (TPV), as detailed in Table 5. The TAP regeneration process induced significant structural changes. During the oxidation step, PFOA was effectively removed; however, the CNT fiber structure was altered, resulting in agglomeration. After resaturation, no further significant changes in the CNT structure were observed.

4. Conclusions

In this work, CM were synthesized from olive oil production and HDPE residues. Of these, HC, AC, and CNT demonstrated significant adsorption capacity for PFOA, with AC outperforming due to its extensive microporous structure and large specific surface area. While HC and CNT showed lower uptake capacities attributable to smaller surface areas. TAP regeneration proved highly effective in restoring the adsorption capacity of saturated materials with PFOA. This methodology was validated experimentally: the final aqueous phase analysis indicated the generation of sulfate and fluoride ions as a result of PS oxidation and PFOA degradation. Agreement between experimental and theoretical sulfate concentrations supported the process's reliability, while partial retention of fluoride ions within the materials was suggested by lower-than-expected measured values. Among the materials tested, AC achieved the highest recovery of adsorption capacity with the lowest persulfate consumption, indicating superior efficiency across adsorption-regeneration cycles. AC also demonstrated excellent structural stability, exhibiting only minor reductions in micropore volume and surface area even after multiple regeneration steps. In contrast, HC and CNT, although they could be regenerated, required higher persulfate doses, experienced notable decreases in micropore surface area, and, for CNT, agglomeration of fibers altered their structural integrity. Importantly, these findings were derived from trials involving higher-than-standard concentrations of PFOA, underlining the robustness and promise of these waste-derived materials for real-world water treatment. Nevertheless, continued research is needed to confirm their effectiveness for adsorption and regeneration in real water matrices and throughout multiple regeneration cycles. The valorization of waste raw materials such as sewage sludge, urban organic residues, and industrial by-products further highlights the importance of sustainable pathways for producing efficient adsorbents. Collectively, this work paves the way for the integration of waste valorization with advanced water treatment technologies, contributing directly to a circular economy and sustainable environmental management. The promising results achieved here indicate real potential for scalable, impactful solutions to pressing environmental challenges.

CRediT authorship contribution statement

Ana Paula Ferreira: Writing – review & editing, Methodology, Investigation, Formal analysis. **Aurora Santos:** Writing – review & editing, Writing – original draft, Supervision, Methodology, Investigation, Funding acquisition, Formal analysis, Data curation, Conceptualization. **Andrés Sánchez-Yepes:** Writing – review & editing, Writing – original draft, Methodology, Investigation, Formal analysis. **Arturo Romero:** Writing – review & editing, Supervision, Investigation. **Helder T. Gomes:** Writing – review & editing, Writing – original draft, Supervision, Methodology, Investigation, Funding acquisition, Formal analysis, Data curation, Conceptualization. **David Lorenzo:** Writing – review & editing, Writing – original draft, Supervision, Software, Methodology, Investigation, Formal analysis, Data curation, Conceptualization.

Declaration of Competing Interest

The authors declare that they have no known competing financial interests or personal relationships that could have appeared to influence the work reported in this paper.

Acknowledgement

This research is part of the project PID2022–137828OB-I00 (EMULREM) funded by MCIN/AEI/10.13039/501100011033. The Community of Madrid also funded this project through the project CARESOIL-CM (TEC2024/ECP-60. A.S.-Y. would like to thank the Ministry of Science and Innovation for supporting predoctoral contracts under FPI grant PRE2020–093195 and Grants for stays in R&D Centres BDNS Identify 525644. The authors are also grateful to the Foundation for Science and Technology (FCT, Portugal) for the financial support through national funds by FCT/MCTES (PIDDAC): CIMO, UIDB/00690/2020 (DOI: 10.54499/UIDB/00690/2020) and UIDP/00690/2020 (DOI:10.54499/UIDP/00690/2020); and SusTEC, LA/P/0007/2020 (DOI:10.54499/LA/P/0007/2020). Ana Paula Ferreira thanks her doctoral Grant with reference PRT/BD/153090/2021, financed by FCT, with funds from NORTE2020, under Program MIT Portugal.

Data availability

No data was used for the research described in the article.

References

[1] V.K. Gaur, P. Sharma, R. Sirohi, M.K. Awasthi, C.-G. Dussap, A. Pandey, Assessing the impact of industrial waste on environment and mitigation strategies: a comprehensive review, J. Hazard. Mater. 398 (2020) 123019.

[2] K. Priti, Mandal, Review on evolution of municipal solid waste management in India: practices, challenges and policy implications, J. Mater. Cycles Waste Manag. 21 (2019) 1263–1279.

[3] X. Yuan, P.D. Dissanayake, B. Gao, W.-J. Liu, K.B. Lee, Y.S. Ok, Review on upgrading organic waste to value-added carbon materials for energy and environmental applications, J. Environ. Manag. 296 (2021) 113128.

[4] A.U. Zaman, S. Lehmann, Urban growth and waste management optimization towards 'zero waste city, City Cult. Soc. 2 (2011) 177–187.

[5] H. Takiguchi, Global Environment Facility's support for sustainable waste management, J. Mater. Cycles Waste Manag. 18 (2016) 248–257.

[6] N. Islam, M. Sandanayake, S. Muthukumaran, D. Navaratna, Review on sustainable construction and demolition waste management-challenges and research prospects, Sustainability 16 (2024).

[7] X.Z. Yuan, Y. Cao, J. Li, A.K. Patel, C.D. Dong, X. Jin, C. Gu, A.C.K. Yip, D.C. W. Tsang, Y.S. Ok, Recent advancements and challenges in emerging applications of biochar-based catalysts, Biotechnol. Adv. 67 (2023).

[8] J. Singh, M. Verma, Waste derived modified biochar as promising functional material for enhanced water remediation potential, Environ. Res. 245 (2024).

[9] M. Kumar, S.K. Bhujbal, K. Kohli, R. Prajapati, B.K. Sharma, A.D. Sawarkar, K. Abhishek, S. Bolan, P. Ghosh, M.B. Kirkham, L.P. Padhye, A. Pandey, M. Vithanage, N. Bolan, A review on value-addition to plastic waste towards achieving a circular economy, Sci. Total Environ. 921 (2024) 171106.

[10] N. Muttil, S. Jagadeesan, A. Chanda, M. Duke, S.K. Singh, Production, TYpes, and Applications of Activated Carbon Derived from Waste Tyres: an overview, Appl. Sci. Basel 13 (2023).

[11] N. Hardyanti, H. Susanto, F.A. Kusuma, M.A. Budihardjo, A bibliometric review of adsorption treatment with an adsorbent for wastewater, Pol. J. Environ. Stud. 32 (2023) 981–989.

[12] A.A. Thamer, A. Mustafa, H.Q. Bashar, B. Van, P.-C. Le, M. Jakab, T.R. Rashed, K. Kulacz, M. Hathal, V. Somogyi, D.D. Nguyen, Activated carbon and their nanocomposites derived from vegetable and fruit residues for water treatment, J. Environ. Manag. 359 (2024) 121058.

[13] B. Chemani, K. Benrachedi, The preparation of activated carbons from olive mill waste water by chemical and physical activation, International Multidisciplinary Scientific GeoConference Surveying Geology and Mining Ecology Management, SGEM, 1 (2013) 1065-1072.

[14] G. Enaime, K. Ennaciri, A. Ounas, A. Bacaoui, M. Seffen, S. Taher, A. Yaacoubi, Preparation and characterization of activated carbons from olive wastes by physical and chemical activation: Application to Indigo carmine adsorption, J. Mater. Environ. Sci. 8 (2017) 4125–4137.

[15] E. Diaz, I. Sanchis, C.J. Coronella, A.F. Mohedano, Activated carbons from hydrothermal carbonization and chemical activation of olive stones: application in sulfamethoxazole adsorption, Resources 11 (2022) 43.

[16] N. Dutta, A. Gupta, Characterization and use of waste plastic char for removal of arsenic and COD from aqueous solution, Int. J. Environ. Sci. Technol. 20 (2023) 7735–7748.

[17] Olive Oil Council. Available online: ⟨http://www.internationaloliveoil.org/estaticos/view/131-world-olive-oil-figures⟩ (accessed on 4 June 2024).

[18] M.A. Nunes, F.B. Pimentel, A.S.G. Costa, R.C. Alves, M.B.P.P. Oliveira, Olive by-products for functional and food applications: challenging opportunities to face environmental constraints, Innov. Food Sci. Emerg. Technol. 35 (2016) 139–148.

[19] F. Fornes, R.M. Belda, P. Fernández de Córdova, J. Cebolla-Cornejo, Assessment of biochar and hydrochar as minor to major constituents of growing media for containerized tomato production, J. Sci. Food Agric. 97 (2017) 3675–3684.

[20] S. Kang, X. Li, J. Fan, J. Chang, A direct synthesis of adsorbable hydrochar by hydrothermal conversion of lignin, Energy Sources Part A Recovery Util. Environ. Eff. 38 (2016) 1255–1261.

[21] L. Lebreton, A. Andrady, Future scenarios of global plastic waste generation and disposal, Palgrave Commun. 5 (2019) 6.

[22] H. Gim, J.H. Park, W.Y. Choi, J. Yang, D. Kim, K.-H. Lee, J.W. Lee, Plastic waste residue-derived boron and nitrogen co-doped porous hybrid carbon for a modified separator of a lithium sulfur battery, Electrochim. Acta 380 (2021) 138243.

[23] M. Martin-Martinez, B.F. Machado, P. Serp, S. Morales-Torres, A.M.T. Silva, J. L. Figueiredo, J.L. Faria, H.T. Gomes, Carbon nanotubes as catalysts for wet peroxide oxidation: The effect of surface chemistry, Catal. Today 357 (2020) 332–340.

[24] L.C. Ge, M.J. Zuo, Y. Wang, R.K. Wang, N. Rong, Z.F. Qi, C. Zhao, Y.L. Zhang, C. Xu, A review of comprehensive utilization of biomass to synthesize carbon nanotubes: From chemical vapor deposition to microwave pyrolysis, J. Anal. Appl. Pyrolysis (2024) 177.

[25] J.L. Diaz de Tuesta, B.F. Machado, P. Serp, A.M.T. Silva, J.L. Faria, H.T. Gomes, Janus amphiphilic carbon nanotubes as Pickering interfacial catalysts for the treatment of oily wastewater by selective oxidation with hydrogen peroxide, Catal. Today 356 (2020) 205–215.

[26] F.F. Roman, L. De Grande Piccinin, A.Santos Silva, J.L. Diaz de Tuesta, I.V. K. Freitas, A. Vieira, G. Gonçalves Lenzi, A. Manuel Tavares Silva, J.L. Faria, H. T. Gomes, Carbon Nanomaterials from Polyolefin Waste: Effective Catalysts for Quinoline Degradation through Catalytic Wet Peroxide Oxidation, Catalysts 13 (2023) 1259.

[27] F.E. Titchou, H. Zazou, H. Afanga, J. El Gaayda, R.A. Akbour, M. Hamdani, Removal of Persistent Organic Pollutants (POPs) from water and wastewater by adsorption and electrocoagulation process, Groundw. Sustain. Dev. 13 (2021).

[28] H.M. Mbuvi, Adsorption kinetics and isotherms of methylene blue by geopolymers derived from common clay and rice husk ash, Phys. Chem. 7 (2017) 87–97.

[29] N. Jagadeesh, B. Sundaram, Adsorption of pollutants from wastewater by biochar: a review, J. Hazard. Mater. Adv. 9 (2023) 100226.

[30] J.R. Beaumont, L.M. Pedersen, B.D. Whitaker, 5 - Production and operations management, in: J.R. Beaumont, L.M. Pedersen, B.D. Whitaker (Eds.), Managing the Environment, Butterworth-Heinemann, Oxford, 1993, pp. 141–178.

[31] W.-S. Chen, C.-W. Lin, F.-C. Chang, W.-J. Lee, J.-L. Wu, Utilization of spent activated carbon to enhance the combustion efficiency of organic sludge derived fuel, Bioresour. Technol. 113 (2012) 73–77.

[32] P.M. Álvarez, F.J. Beltrán, V. Gómez-Serrano, J. Jaramillo, E.M. Rodríguez, Comparison between thermal and ozone regenerations of spent activated carbon exhausted with phenol, Water Res. 38 (2004) 2155–2165.

[33] G.D. Okwadha, J. Li, B. Ramme, D. Kollakowsky, D. Michaud, Thermal removal of mercury in spent powdered activated carbon from Toxecon process, J. Environ. Eng. 135 (2009) 1032–1040.

[34] X. Huang, D. An, J. Song, W. Gao, Y. Shen, Persulfate/electrochemical/FeCl2 system for the degradation of phenol adsorbed on granular activated carbon and adsorbent regeneration, J. Clean. Prod. 165 (2017) 637–644.

[35] O. Zanella, I.C. Tessaro, L.A. Féris, Desorption- and decomposition-based techniques for the regeneration of activated carbon, Chem. Eng. Technol. 37 (2014) 1447–1459.

[36] S. Parsons, Advanced Oxidation Processes for Water and Wastewater Treatment, IWA Publishing, 2005.

[37] A.V. Baskar, N. Bolan, S.A. Hoang, P. Sooriyakumar, M. Kumar, L. Singh, T. Jasemizad, L.P. Padhye, G. Singh, A. Vinu, B. Sarkar, M.B. Kirkham, J. Rinklebe, S. Wang, H. Wang, R. Balasubramanian, K.H.M. Siddique, Recovery, regeneration and sustainable management of spent adsorbents from wastewater treatment streams: a review, Sci. Total Environ. 822 (2022) 153555.

[38] A. Sánchez-Yepes, A. Santos, J.M. Rosas, J. Rodríguez-Mirasol, T. Cordero, D. Lorenzo, Sustainable reuse of toxic spent granular activated carbon by heterogeneous fenton reaction intensified by temperature changes, Chemosphere 341 (2023) 140047.

[39] A. Sanchez-Yepes, A. Santos, J.M. Rosas, J. Rodriguez-Mirasol, T. Cordero, D. Lorenzo, Regeneration oF Granulated Spent Activated Carbon with 1,2,4-trichlorobenzene using thermally activated persulfate, Ind. Eng. Chem. Res 61 (2022) 9611–9620.

[40] T. Stahl, D. Mattern, H. Brunn, Toxicology of perfluorinated compounds, Environ. Sci. Eur. 23 (2011) 38.

[41] A. Santos, S. Rodríguez, F. Pardo, A. Romero, Use of Fenton reagent combined with humic acids for the removal of PFOA from contaminated water, Sci. Total Environ. 563-564 (2016) 657–663.

[42] I.T. Cousins, R. Vestergren, Z. Wang, M. Scheringer, M.S. McLachlan, The precautionary principle and chemicals management: The example of perfluoroalkyl acids in groundwater, Environ. Int. 94 (2016) 331–340.

[43] A. Bhakhri, J. Bliss, T. Finelli, S. Kurrumchand, K. Roberts, Z. Wang, Removal of PFOA from water using UV treatment, chemical oxidation, & adsorption by activated carbon & zeolites, BS. Major Qualify Project, Worcester Polytechnic Institute, (2012).

[44] J. Cheng, L. Huang, Y. Li, Z. Zhang, R. Mu, C. Liu, S. Hu, Y. Xiao, M. Xu, A review of treatment technologies for perfluorooctane sulfonate (PFOS) and perfluorooctanoic acid (PFOA) in water, Processes 11 (2023) 2260.

[45] J. Xu, Z. Liu, D. Zhao, N. Gao, X. Fu, Enhanced adsorption of perfluorooctanoic acid (PFOA) from water by granular activated carbon supported magnetite nanoparticles, Sci. Total Environ. 723 (2020) 137757.

[46] J. Petrović, M. Ercegović, M. Simić, M. Koprivica, J. Dimitrijević, A. Jovanović, J. Janković Pantić, Hydrothermal carbonization of waste biomass: a review of hydrochar preparation and environmental application, Processes 12 (2024) 207.

[47] B. Saawarn, B. Mahanty, S. Hait, Adsorptive removal of perfluorooctanoic acid from aqueous matrices using peanut husk-derived magnetic biochar: statistical and artificial intelligence approaches, kinetics, isotherm, and thermodynamics, Chemosphere 360 (2024) 142397.

[48] M. Ahmad, A.U. Rajapaksha, J.E. Lim, M. Zhang, N. Bolan, D. Mohan, M. Vithanage, S.S. Lee, Y.S. Ok, Biochar as a sorbent for contaminant management in soil and water: a review, Chemosphere 99 (2014) 19–33.

[49] S. Jatta, S. Huang, C. Liang, A column study of persulfate chemical oxidative regeneration of toluene gas saturated activated carbon, Chem. Eng. J. 375 (2019) 122034.

[50] J. Peng, E. Wu, N. Wang, X. Quan, M. Sun, Q. Hu, Removal of sulfonamide antibiotics from water by adsorption and persulfate oxidation process, J. Mol. Liq. 274 (2019) 632–638.

[51] P.-f Xiao, L. An, D.-d Wu, The use of carbon materials in persulfate-based advanced oxidation processes: a review, N. Carbon Mater. 35 (2020) 667–683.

[52] S.G. Huling, S. Ko, S. Park, E. Kan, Persulfate oxidation of MTBE- and chloroform-spent granular activated carbon, J. Hazard. Mater. 192 (2011) 1484–1490.

[53] A. Bhattarai, M. Khanal, D. Rai, R. Khanal, Determination of point zero charge (PZC) of homemade charcoals Of Shorea robusta (Sakhuwa) and pinus roxburghii (Salla), Int. J. Eng. Res. Technol. 9 (2020).

[54] M. Lu, G. Cagnetta, K. Zhang, J. Huang, G. Yu, Mechanochemical mineralization of "very persistent" fluorocarbon surfactants - 6:2 fluorotelomer sulfonate (6:2FTS) as an example, Sci. Rep. 7 (2017) 17180.
[55] E. Jurado, M. Fernández-Serrano, J. Núñez-Olea, G. Luzón, M. Lechuga, Simplified spectrophotometric method using methylene blue for determining anionic surfactants: applications to the study of primary biodegradation in aerobic screening tests, Chemosphere 65 (2006) 278–285.
[56] V. Ţucureanu, A. Matei, A.M. Avram, FTIR spectroscopy for carbon family study, Crit. Rev. Anal. Chem. 46 (2016) 502–520.
[57] P.K. Chu, L. Li, Characterization of amorphous and nanocrystalline carbon films, Mater. Chem. Phys. 96 (2006) 253–277.
[58] M.D. Donohue, G.L. Aranovich, Classification of Gibbs adsorption isotherms, Adv. Colloid Interface Sci. 76-77 (1998) 137–152.
[59] K.S.W. Sing, Reporting physisorption data for gas/solid systems with special reference to the determination of surface area and porosity (Recommendations 1984), Pure Appl. Chem. 57 (1985) 603–619.
[60] K.S.W. Sing, Physisorption of gases by carbon blacks, Carbon 32 (1994) 1311–1317.
[61] S.-K. Ahn, K.-Y. Park, W.-j Song, Y.-m Park, J.-H. Kweon, Adsorption mechanisms on perfluorooctanoic acid by FeCl3 modified granular activated carbon in aqueous solutions, Chemosphere 303 (2022) 134965.
[62] A. Sánchez-Yepes, A. Santos, J.M. Rosas, J. Rodríguez-Mirasol, T. Cordero, D. Lorenzo, Regeneration of Granulated Spent Activated Carbon with 1,2,4-Trichlorobenzene Using Thermally Activated Persulfate, Ind. Eng. Chem. Res. 61 (2022) 9611–9620.
[63] D. Zhang, Q. Luo, B. Gao, S.-Y.D. Chiang, D. Woodward, Q. Huang, Sorption of perfluorooctanoic acid, perfluorooctane sulfonate and perfluoroheptanoic acid on granular activated carbon, Chemosphere 144 (2016) 2336–2342.
[64] P.-J. Huang, M. Hwangbo, Z. Chen, Y. Liu, J. Kameoka, K.-H. Chu, Reusable Functionalized Hydrogel Sorbents for Removing Long- and Short-Chain Perfluoroalkyl Acids (PFAAs) and GenX from Aqueous Solution, ACS Omega 3 (2018) 17447–17455.
[65] T. Yan, H. Chen, F. Jiang, X. Wang, Adsorption of perfluorooctane sulfonate and perfluorooctanoic acid on magnetic mesoporous carbon nitride, J. Chem. Eng. Data 59 (2014) 508–515.
[66] B.K. Pradhan, N.K. Sandle, Effect of different oxidizing agent treatments on the surface properties of activated carbons, Carbon 37 (1999) 1323–1332.
[67] S. Sukeesan, S.K. Boontanon, N. Boontanon, S. Fujii, Regeneration of ion-exchange resins and granular activated carbon with the sonochemical technique for enabling adsorption of aqueous per- and polyfluoroalkyl substances, IOP Conference Series Earth Environmental Science 973 (2022) 012004.
[68] M. Forouzesh, A. Ebadi, A. Aghaeinejad-Meybodi, R. Khoshbouy, Transformation of persulfate to free sulfate radical over granular activated carbon: effect of acidic oxygen functional groups, Chem. Eng. J. 374 (2019) 965–974.
[69] M. Forouzesh, A. Ebadi, A. Aghaeinejad-Meybodi, Degradation of metronidazole antibiotic in aqueous medium using activated carbon as a persulfate activator, Sep. Purif. Technol. 210 (2019) 145–151.